Industrial Crops & Products 188 (2022) 115668

Contents lists available at ScienceDirect

Industrial Crops & Products

journal homepage: www.elsevier.com/locate/indcrop

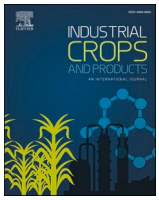

Improvement of the barrier and mechanical properties of environmentally friendly mango kernel flour/glycerol films by varying the particle size of mango kernel flour

Jaume Gomez-Caturla [a,*], Juan Ivorra-Martinez [a], Luis Quiles-Carrillo [a], Rafael Balart [a], Daniel Garcia-Garcia [a], Franco Dominici [b], Debora Puglia [b], Luigi Torre [b]

[a] Instituto de Tecnología de Materiales (ITM), Universitat Politècnica de València (UPV), Plaza Ferrándiz y Carbonell 1, 03801 Alcoy, Alicante, Spain
[b] Dipartimento di Ingegneria Civile ed Ambientale, University of Perugia, UdR INSTM, Strada di Pentima, 4, 05100 Terni, TR, Italy

ARTICLE INFO

Keywords:
Mango kernel flour
Biodegradability
Antioxidant
Glycerol
Film

ABSTRACT

The development of environmentally friendly films based on glycerol and different sizes of mango kernel flour particles (MKF), ranging from 100 to 600 μm, is reported. The casting solution method was used to produce the films, using distilled water as the solvent. The mechanical, morphological, barrier, surface, optical, wettability and biodegradability properties of the films were assessed. The mechanical analysis revealed that smaller particles lead to superior mechanical performance in terms of tensile strength, elastic modulus and elongation at break, achieving an elongation at break of 18.1 % for the films with the smallest particle size (100 μm). These results were confirmed by field emission scanning electron microscopy (FESEM) images of the films, where the gap between the mango kernel particles and the glycerol matrix is practically non-existent in films with the smallest particle size (100 μm). On the other hand, it was observed that as the particle size decreased, the barrier properties improved, showing a decrease in water vapor permeability rate (WVPR). With respect to antioxidant properties, it was observed that the films showed strong antioxidant activity, as assessed by 2,2–diphenyl–1–picrylhydrazyl (DPPH) inhibition above 90 % for all films after 1 week. Finally, MKF films proved to be completely biodegradable, with a 100 % of disintegration after 4 weeks of incubation time in compost soil, with the smallest MKF particle size films exhibiting the highest disintegration rate.

1. Introduction

In the last few decades, the production of plastics all over the globe has risen up considerably. Most of those plastics are based on fossil-resources, which provoke several environmental problems, such as large amount of wastes or greenhouse gas emissions (Shen et al., 2020). In addition, the petroleum used to produce these plastics has suffered a noticeable depletion since the 20th century. Among all the industries, the packaging industry stands out as the main consumer, which accounts for the 36 % of the total plastic production (approximately 400 million ton per year) (Jang et al., 2020). This fact has led society to concern about environmentally friendly alternatives as substitutes for traditional synthetic plastics (Liminana et al., 2018). Among all the environmentally friendly materials that are being developed in search for better alternatives in food packaging, edible films and coatings obtained from biopolymers, especially polysaccharides and proteins, have attracted great interest (Ghiasi et al., 2020). Biopolymeric films find important applications in the food industry thanks to their ability to provide protection to food products against mechanical damage and adverse effects of microbiological, chemical, and physical origin (Giosafatto et al., 2018). Additionally, these films are characterized by their low cost, wide availability and biodegradability (Kocabaş et al., 2021; Zhang et al., 2016).

Proteins, polysaccharides and lipids are the most common used biopolymers for biodegradable films preparation. Some examples are protein films, which possess good barrier properties against lipids, aromas and oxygen under low relative humidity environments (Bamdad et al., 2006), but they are poor water vapor barriers because of their hydrophilicity (Mokrejs et al., 2009). There are also starch films, which have balanced tensile strength and good oxygen barrier properties, but they are also very sensitive to moisture and become very brittle in low humidity atmospheres (Li et al., 2018; Wang et al., 2021b). To overcome

* Corresponding author.
E-mail address: jaugoca@epsa.upv.es (J. Gomez-Caturla).

https://doi.org/10.1016/j.indcrop.2022.115668
Received 5 April 2022; Received in revised form 24 August 2022; Accepted 13 September 2022
Available online 20 September 2022

these weaknesses, some studies have focused on developing blends of commercial starch and protein to make films (Huntrakul et al., 2020). In some cases, lipids have been added in order to reduce the hydrophilicity of the blends and increase the water vapor barrier properties of the obtained films (Colla et al., 2006). However, results are not always optimal, due to possible incompatibility between the biopolymers during blending, which could provoke phase separation (Grinberg and Tolstoguzov, 1997). Nonetheless, in order to sort out this problem, composite films are also an interesting solution, where flours or micronizates from raw materials coming from plants such as cereals, fruits or other vegetables can act as "natural mixtures" of starch, lipids and proteins (Hassan et al., 2018). Several flour-based materials have been studied as film-forming agents. Tapia-Blácido et al. (2011), reported the good film forming ability of amaranth flour in films with glycerol as plasticizer. Other researches have developed films based on eggplant flour, corn starch (Nouraddini et al., 2018) or chia seeds (Dick et al., 2016). However, those films gave poor results, lacking homogeneity and showing low mechanical properties. Mikus et al. (2021), developed and tested several oilseed flours (flax, evening primrose, pumpkin, hemp, sunflower and sesame), as film forming agents, also analyzing the effect of the size of the particles of the different flours. The study showed that the films with highest amount of protein, namely sesame and pumpkin, had the best barrier properties in terms of water vapor permeability. Additionally, Wang et al. (2021a) made a considerable contribution to the cellulose-based packaging investigation route by developing a lignocellulose-derived strategy through the deposition of oxalic acid modified microfibrillated cellulose (OMFC) and infiltration of nanosized alkaili lignin (NAL) in paper packaging. They achieved a great increase in barrier properties (reduction of WVTR of 93 %). Quiles-Carrillo et al. (2019) reported on the development of bioactive multilayer polylactide films with enhanced barrier properties against the diffusion of gallic acid.

Mango (*Mangifera indica*) is one of the most popular tropical crops worldwide. Its production reached 46.5 million metric tons in 2016 (Melo et al., 2019), and India is its main exporter, which represents more than 40% share of the global market (Thakor, 2019). Several studies have demonstrated that mango by-products, like mango peel or mango stone, are potential feedstocks for biorefineries, due to their content in several interesting components, such as starch, cellulose, proteins, polyphenols, and so on (Silva et al., 2019). The mango seed is divided into two main components, the kernel (interior) and the tegument (exterior). Mango kernel represents about the 13 wt% of Tommy Atkins mangoes variety, which is the predominant one (Bally et al., 2021), and it can be utilized as a supplement to wheat flour or for extracting edible oil (Yatnatti et al., 2014). The main component of mango kernels is starch. According to previous studies, mango kernel has around 74–75 wt% of polysaccharides with starch accounting for 60 wt%. Other components of the mango kernel are 9–13 wt% fats, 6–9 wt% proteins, and 2–3 wt% ashes as shown by Augustin and Ling (1987). It even has phenolic compounds, as it was demonstrated by Adilah et al. (2018b). All these compounds make mango kernel an excellent option to be considered for producing edible films.

When producing edible coatings and films, barrier properties and mechanical properties are essential. In this sense, the particle size of the flour plays a key role in those properties. However, little research has been done with regard to the different behavior of edible films based on the particle size of the film-forming agent flour. Pérez-Gago and Krochta (2001), conducted an study on how the lipid particle size affected the water vapor permeability (WVP) of films based on whey protein/Beeswax emulsion, and observed that smaller particles lead to better barrier and mechanical properties. This fact suggests that it would be of interest to study how particle size of starch-based flours would affect the properties of films. Another important characteristic considering films focused on food packaging applications is their antioxidant activity. Lipid oxidation consists on a radical chain reaction that affects food with high concentration of unsaturated lipids, which results in the release of free radicals and volatiles that produce oxidative rancidity (Melo et al., 2019). Antioxidants respond to this reaction by scavenging those free radicals and donating hydrogen atoms to free radicals, thus delaying or even stopping the chain reaction. Melo et al. (2019), reported the positive radical scavenging activity of mango kernel flour and phenolic extracts from mango kernel flour in edible antioxidant films.

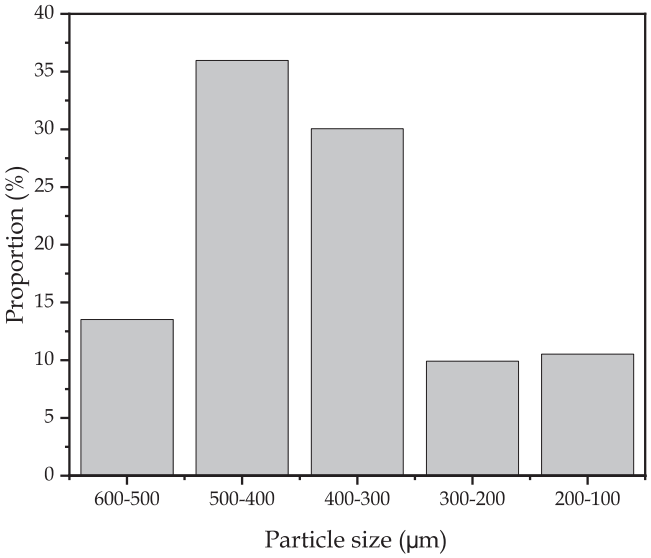

Fig. 1. Particle size distribution of milled mango kernel flour (MKF) after sieving at different size ranges.

The main aim of this study is to obtain environmentally friendly films based on mango kernel flour (MKF) with several particle sizes and glycerol as plasticizer. Thus, the objective is to assess how the particle size affects the properties of the films and which is the size threshold at which films with balanced properties for use in the packaging sector are obtained. To meet this end, five different particle size ranges have been studied (600–500 μm, 500–400 μm, 400–300 μm, 300–200 μm and 200–100 μm). The mechanical, morphological, barrier, colorimetric, biodegradability, moisture and water solubility, contact angle and antioxidant properties have been characterized and evaluated in order to compare the effect of the particle size. Considering that a similar analysis has not been reported before in literature with regard to starch-based flours, the authors deem that this study could be of considerable usefulness for the packaging industry to improve the quality and performance of starch-based films.

2. Materials and methods

2.1. Materials

Osteen variety mangoes were obtained from the local market in Alcoy, Spain. The fruits were selected according to their appearance, so they had no apparent infection. Glycerol was provided by Sigma-Aldrich, and it was ReagentPlus > 99.0 % (Product Code: G7757-1GA). 2,2-diphenyl-1-picrylhydrazyl radical (DPPH) was supplied by Sigma Aldrich (Madrid, Spain). DPPH is a stable organic radical that presents a strong hydrogen acceptor capacity towards antioxidants. In the presence of antioxidants, the characteristic violet color of DPPH solution in methanol changes into yellow. Methanol (≥ 99.8 %) of HPLC grade was supplied by Panreac Química (Barcelona, Spain).

2.2. Mango kernel particles preparation

Mango kernels were first dried at 50 °C during 168 h in a dehumidifying dryer MDEO (Barcelona, Spain). They were then decorticated and cut into small pieces using an air knife unit. Afterwards, they were

Table 1
Code for the developed films with different MKF particle size.

Code	Composition
MKF-600/500	Film with MKF particles with a size between 600 and 500 μm
MKF-500/400	Film with MKF particles with a size between 500 and 400 μm
MKF-400/300	Film with MKF particles with a size between 400 and 300 μm
MKF-300/200	Film with MKF particles with a size between 300 and 200 μm
MKF-200/100	Film with MKF particles with a size between 200 and 100 μm

milled in a ZM 200 centrifugal mill from Retsch (Düsseldorf, Germany) at a speed of 12,000 rpm and sieved with a 500-μm mesh filter. Finally, in order to evaluate the behavior of the films with different particle size, the mango kernel flour (MKF) was sieved using a vibratory sieve shaker model RP09 from CISA (Barcelona, Spain) through several mesh sizes: 600, 500, 400, 300, 200 and 100 μm. This allowed to separate the flour in different particle size sets. Fig. 1 illustrates the proportion of each particle size in the milled MKF. It can be observed how the most abundant range is 500–400 μm, which was expected as the initial mesh size was 500 μm. According to Adjei-Fremah et al. (2019), the particle size distribution is a decisive factor regarding the functional properties of the films, particularly the hydration properties, which are greatly influenced by porosity.

2.3. Preparation of reinforced MKF/glycerol films

The MKF/glycerol films were prepared by solution casting process using MKF, glycerol and distilled water. For this purpose, MKF (5 % w/w) of each particle size set was mixed with distilled water. After stirring for 10 min, the mixture was heated up to 90 °C and stirred for 30 min. Afterwards, glycerol was added to the mixture (50 % w/w in relation to the MKF mass) as a plasticizer, and the solution was stirred for 30 min once more. Then the solutions were ultrasonicated with an ultrasonicator model MH-010S from Valens (Palma de Mallorca, Spain) for 10 min with the objective of removing bubbles. The solutions were thereafter casted onto Petri plates (8.5 cm diameter) and allowed to dry in a dehumidifying dryer MDEO for 48 h at 40 °C. Finally, the dried films were extracted from the Petri plates and stored at 52 % relative humidity (RH) at 25 °C for 48 h before characterization. Three films from each formulation were prepared. The nomenclature for the prepared films is shown in Table 1.

2.4. Characterization of MKF/glycerol films

2.4.1. Film thickness

Film thickness was determined using a micrometer Mitutoyo No. 2109S-10 (Tokyo, Japan) with a sensitivity of 0.001 mm. Ten measurements were made all along the surface of each film sample.

2.4.2. Mechanical properties

The mechanical tensile properties, namely tensile strength, tensile modulus and elongation at break of MKF/glycerol films were determined following ASTM D882-02, using a tensile machine model DUOTRAC-10/1200 from ibertest (Madrid, Spain). Rectangular strips (30×4 mm^2) were cut from preconditioned MKF/glycerol films and placed between the tensile grips with a distance of 15 mm. The crosshead speed during the test was 5 mm/min. Five samples from each film were used for the tensile test in order to obtain the average results.

2.4.3. Moisture content

The moisture of MKF/glycerol films was determined gravimetrically. 10×10 mm^2 film pieces were cut and weighted, then they were dried in an oven for 24 h at 105 °C and weighted again until reaching a constant weight (Tonyali et al., 2018). Three pieces from each film were used to calculate the moisture content and the results were averaged. The moisture content for each sample was obtained through Eq. (1):

$$\text{Moisture content}(\%) = \frac{W_i - W_f}{W_i} 100 \quad (1)$$

where W_i and W_f are the initial and dried weight of the samples, respectively.

2.4.4. Morphology

Nitrogen cryofractured cross-sections of MKF/glycerol films were used to study their morphology by means of field emission scanning electron microscopy (FESEM). A ZEISS model ULTRA55 (Eindhoven, The Netherlands) was used. The acceleration voltage was 2 kV The film samples were sputtered with a platinum coating in a high vacuum sputter coater EM MED20 from Leica Microsystems (Milton Keynes, United Kingdom).

2.4.5. Solubility

The solubility of MKF/glycerol film samples in distilled water was calculated following the methodology of Masamba et al. (2016). Rectangular pieces of the films (10×10 mm^2) were dried in an oven for 24 h at 105 °C. They were then weighted and the film pieces were placed into test tubes with approximately 10 mL of distilled water. The tubes were submitted to periodical agitation for 24 h at room temperature. Then, the non-solubilized fraction was dried in an oven 24 h at 105 °C with the aim of determining the weight of undissolved dry matter in distilled water. Solubility was calculated according to Eq. (2):

$$\text{Solubility}(\%) = \frac{W_i - W_f}{W_i} 100 \quad (2)$$

where W_i is the initial weight of the sample, and W_f is the weight of the sample after drying. Three measurements were made for each film.

2.4.6. Dynamic contact angle measurements

Dynamic water contact angles (θ) of preconditioned films were measured using an optical goniometer model FM140 (110/220 V, 50/60 Hz) from KRÜSS GmbH (Hamburg, Germany) at room temperature. Five distilled water drops were placed in the surface of the films and their contact angle was measured. Ten measurements for each water droplet were taken and averaged. The contact angle was measured at different times from the deposition of the water drop onto the film surface (0, 5, 10, 20, 30 s), thus obtaining the dynamic water contact angle.

2.4.7. Color characterization

The change in color produced by MKF in the glycerol films was assessed using a colorimeter model KONICA CM-3600d COLORFLEX-DIFF2 from Hunter Associates Laboratory (Virginia, EEUU). A white standard was used to calibrate the equipment. Color analysis of each film was carried out through the study of the CIELab color space, whose coordinates are L^* (lightness), a^* (red-green) and b^* (yellow-blue). The results were obtained by averaging five measurements at ten random points of each film. The total difference in color (ΔE) was obtained using Eq. (3):

$$\Delta E = \sqrt{(\Delta L^*)^2 + (\Delta a^*)^2 + (\Delta b^*)^2} \quad (3)$$

where ΔL^*, Δa^* and Δb^* are the differences between the corresponding color parameter of the samples and the color parameter values of the white standard plate ($L^* = 95.17$, $a^* = -0.93$, $b^* = 0.53$).

2.4.8. Water vapor transmission rate (WVTR)

MKF/glycerol films' water vapor transmission rate (WVTR) was measured gravimetrically according to ISO 2525. First, permeability cups were filled with 2 g of dry silica gel; then they were sealed with film samples and placed in a desiccator at 90 % relative humidity (RH) and 23 °C. The cups were weighted each hour for 7 h. The changes in the

weight of the cup were plotted as a function of time and their slope was obtained through linear regression. WVTR was calculated using Eq. (4) (Trifol et al., 2016):

$$\mathrm{WVTR} = \frac{\mathrm{n}\cdot\mathrm{l}}{\mathrm{S}} \tag{4}$$

where n is the slope obtained by linear regression, l is the thickness of the film and S is the exposed area of the film.

2.4.9. Antioxidant activity

The antioxidant activity of MKF/glycerol films was assessed using 2,2-diphenyl-1-picrylhydrazyl radical (DPPH) inhibition test. DPPH is a stable organic radical that presents a strong hydrogen acceptor capacity towards antioxidants. In the presence of antioxidants, the characteristic violet color of DPPH solution in methanol changes into yellow. This color change was measured by means of UV spectrophotometry. A standard DPPH solution with a concentration of 0.025 g/L in methanol was prepared and placed in dark glass vials. ≈ 100 mg samples from each film were prepared and immersed in 4 mL of the standard solution. Vials containing all the samples and a control were closed and kept away from light for one week.

An Agilent Technologies (Barcelona, Spain) Cary series UV-Vis-NIR spectrophotometer was used to measure the absorbance of the samples at 517 nm, at 1, 24, 72, and 168 h after the start of the test, in triplicate. The percentage inhibition of DPPH was calculated according to Eq. (5):

$$\mathrm{DPPH}_{\mathrm{inhibition}}(\%) = \frac{\mathrm{A_c} - (A_s - A_b)}{\mathrm{A_c}} \quad 100 \tag{5}$$

where A_C is the absorbance of the DPPH solution without the sample, A_s is the absorbance of the DPPH solution with the sample, and A_b is the absorbance value of pure methanol with the sample. Tests were done by triplicate to obtain reliable results.

2.4.10. Disintegration test

The biodegradation rate under controlled compost soil conditions of MKF/glycerol films with different particle sizes of MKF was studied following ISO 20200. Pieces of 2.5 × 2.5 cm^2 were cut from the obtained films and dried for 24 h at 40 °C. Then they were weighted and buried in a bioreactor of dimensions 30 × 20 × 10 cm^3 in a solid synthetic wet soil prepared with 40 wt% sawdust, 10 wt% corn starch, 30 wt% rabbit-feed, 10 wt% compost, 5 wt% sugar, 4 wt% of corn oil, and 1 wt% of urea. This mixture was mixed with distilled water in a 45:55 ratio. In these conditions, the samples were aerobically degraded at a constant temperature of 58 °C in an air circulating oven during 4 weeks. Measurements were taken by extracting samples from the reactor, washing them with distilled water, drying them for 24 h at 40 °C and finally weighting them. The samples were individually placed inside a textile mesh that allows a direct contact with the compost soil during the disintegration period and, at the same time, since the textile mesh does not disintegrate, it facilitates the removal of the degraded film or films pieces to carry out weight measurements as indicated before. Once the weight measurement was done, the film or remaining film pieces were placed again into the textile mesh to continue with the disintegration test. Several measurements were taken during the 4 weeks to observe the biodegradation profile of the samples over time.

2.4.11. Roughness

The surface roughness of the MKF/glycerol films was characterized using a roughness meter Mitutoyo model SJ301. A linear path with a length of 4 mm was studied in each film following ISO1997. The mean surface roughness (R_a) was measured in triplicate for each MKF/glycerol film.

2.4.12. Statistical analysis

To evaluate the significant differences among the samples, a 95 % confidence level ($p \leq 0.05$) by one-way analysis of variance (ANOVA) following Tukey's test was conducted. The software OriginPro 8 (OriginLab Corporation, Northampton, MA, USA) was used to carry out this analysis.

Table 2
Average thickness and mechanical properties of the MKF/glycerol films from tensile test: tensile modulus (E), tensile strength (σ_{max}) and elongation at break (ε_b).

Film	Thickness (μm)	E (MPa)	σ_{max} (MPa)	ε_b (%)
MKF-600/500	528.3 ± 58.4^a	9.85 ± 1.66^a	0.75 ± 0.06^a	11.4 ± 2.1^a
MKF-500/400	511.1 ± 30.2^a	14.42 ± 1.21^b	0.90 ± 0.17^b	11.4 ± 0.9^a
MKF-400/300	520.9 ± 74.8^a	22.40 ± 7.78^c	0.90 ± 0.07^b	11.8 ± 0.3^a
MKF-300/200	474.5 ± 13.8^b	20.07 ± 3.24^d	0.93 ± 0.06^b	15.3 ± 1.0^b
MKF-200/100	420.9 ± 22.8^c	22.10 ± 3.73^e	1.08 ± 0.08^c	18.1 ± 1.2^c

a–e Different letters in the same column indicate a significant difference ($p < 0.05$).

3. Results and discussion

3.1. Mechanical properties

The mechanical properties of the MKF/glycerol films allow to determine how the films behave under tensile stress depending on the difference in particle size. In this sense, Table 2 gathers the main tensile parameters of the films as well as the film thickness. It can be observed how the thickness of the films varies between 420 μm for the smallest MKF particle film, and 528 μm for the largest MKF particle film. This reduction in thickness could be closely ascribed to the particle size. In the case of the 600/500 μm particles film, the particles almost comprise the entirety of the film thickness. The tensile modulus (E) obtained for the film with 600–500 μm MKF particle size was 9.85 MPa, while tensile strength and elongation at break were 0.75 MPa and 11.4 %, respectively. Those values are within the range reported by other studies such as the work by Mikus et al. (2021), who studied several films with different lignocellulosic fillers. They reported elastic modulus values ranging from 1 to 19 MPa, tensile strengths comprised in the 0.6–3.1 MPa range, and elongation at breaks varying from 4 % to 25 %.

It can be clearly seen how a decrease in the particle size promotes a direct improvement in the overall tensile properties of the MKF/glycerol films. The tensile modulus increases up to 22.1 MPa for the film with 200–100 μm MKF particles, which means an increase of 124 % in relation to the 600–500 μm MKF particle size film. A similar trend occurs when analyzing tensile strength and elongation at break. Those parameters boost up to 1.08 MPa and 18.1 % for the MKF-200/100 film, respectively. This means an improvement of 44 % and 58.8 %, respectively, in comparison with the MKF-600/500 film. This increase is mainly ascribed to two factors. First, smaller MKF particles make the films more homogeneous and decrease the number of stress concentration points in the films in comparison with the samples with the highest MKF particles. This is ascribed to a greater concentration of agglomerates due to the higher size of the lignocellulosic particles. Moreover, the size of some of the highest MKF particles (MKF-600/500) can even surpass the thickness of the film. The formation of agglomerates leads to a detriment in the cohesion of the films, thus, increasing the brittleness of the film (Mikus et al., 2021). This also leads to the appearance of considerably large areas where only glycerol is present, as it would be demonstrated by FESEM characterization. Additionally, smaller particle size allows a better particle dispersion over the film surface, making a higher amount of particles to be present in the film, with a higher overall surface area. This directly leads to a superior interaction of the oxygen based molecules present in the particles (mainly starch and protein) with the plasticizer (glycerol), as they have more hydrogen bonding capacity to interact with the plasticizer, which enhances both the tensile strength of the material and its ability to elongate (Basiak et al., 2018).

Table 3
Moisture content and water solubility for MKF/glycerol films.

Code	Moisture content (%)	Water solubility (%)
MKF-600/500	26.7 ± 0.1^{a}	31.2 ± 0.2^{a}
MKF-500/400	27.2 ± 1.1^{a}	31.4 ± 0.4^{a}
MKF-400/300	29.9 ± 0.7^{b}	32.8 ± 0.6^{a}
MKF-300/200	31.0 ± 0.2^{b}	34.7 ± 0.1^{b}
MKF-200/100	28.4 ± 0.1^{c}	$31.3 \pm 0.3^{a,c}$

a–c Different letters in the same column indicate a significant difference ($p < 0.05$).

Table 4
Water contact angle at different times (0, 5, 10, 20 and 30 s) for MKF/glycerol films.

Code\Time	Water contact angle (°)				
	0 s	5 s	10 s	20 s	30 s
MKF-600/500	50.7 ± 0.5^{a}	45.9 ± 0.9^{a}	43.0 ± 0.6^{a}	41.0 ± 0.1^{a}	39.5 ± 0.3^{a}
MKF-500/400	36.9 ± 0.4^{b}	26.6 ± 0.7^{b}	25.8 ± 0.5^{b}	25.5 ± 0.6^{b}	25.3 ± 0.8^{b}
MKF-400/300	31.4 ± 0.5^{c}	24.1 ± 0.8^{c}	13.1 ± 0.6^{c}	13.1 ± 0.3^{c}	13.0 ± 0.6^{c}
MKF-300/200	31.7 ± 0.8^{c}	25.1 ± 0.6^{c}	23.6 ± 0.6^{d}	23.5 ± 1.1^{d}	22.0 ± 0.8^{d}
MKF-200/100	$35.3 \pm 0.7^{b,d}$	34.6 ± 1.2^{d}	$26.2 \pm 1.1^{b,e}$	$25.8 \pm 0.4^{b,e}$	$24.7 \pm 0.8^{b,e}$

a–e Different letters in the same column indicate a significant difference ($p < 0.05$).

3.2. Water susceptibility

Table 3 shows the moisture content and water solubility, while Table 4 gathers the dynamic contact angle results for each one of the films developed in this study. The solubility of all the MKF/glycerol films is quite similar, as it is indicated by the statistical analysis. The MKF-600/500 film shows values of 26.7 % and 31.2 % for moisture and water solubility, respectively; while the MKF-300/200 film exhibits values of 31.0 % and 34.7 %, respectively, which is the only film that exhibited a little higher water solubility. Starch-based MKF particles possess great affinity towards water due to their content in starch (60 wt %) and other highly hydrophilic compounds, such as proteins and carbohydrates (Nawab et al., 2017; Yatnatti et al., 2014). Both proteins and carbohydrates possess hydroxyl groups which can readily interact with hydroxyl groups in glycerol. This increase in moisture and water solubility could be ascribed to the fact that smaller lignocellulosic particles possess higher surface contact area, which leads to a superior interaction with water and thus, a higher concentration of -OH groups can interact with H_2O molecules (Cheng et al., 2006; Godbillot et al., 2006). Additionally, part of this ability to absorb water is also due to the presence of glycerol, which is considered a water-holding agent that contributes to hydrophilicity, as observed by Tapia-Blácido et al. (Tapia-Blácido et al., 2011).

Contact angle measurements of the films over time also show remarkable differences in terms of water affinity. The herein developed films are highly hydrophilic, as the water contact angle is quite inferior to 65°, which is the hydrophilicity threshold according to Vogler (Vogler, 1998). At the initial time, all the contact angles are already quite low, being the highest value 50.7° for the higher particle size film and the lowest 31.4° for the MKF-400/300 film. Moreover, the water contact angle rapidly decreases to even lower values after 30 s. The value for MKF-600/500 decreases down to 39.5°, while the contact angle for MKF-400/300 goes down to 13.0°, which is another proof of the extreme hydrophilicity of these films. There seems to be a trend of reduction of contact angle with smaller particle sizes. This could be ascribed to a higher surface area in films with the smaller particle size, as it has been aforementioned. Furthermore, it could be directly related to roughness, as higher particle size films are considerably rougher than lower particle size films, which are more homogeneous. This homogeneity could provoke a decrease in the water contact angle (Ryan and Poduska, 2008). Fig. 2 perfectly illustrates this effect, which shows the evolution of the shape of the distilled water drop onto the surface of the film MKF-500/400 over time. It can be seen how the drop drastically flattens with time.

In accordance with these results, the films are clearly water soluble. This feat still makes them suitable for packaging applications, especially in the oil packaging field (Rosenbloom and Zhao, 2021). Romero-Bastida et al. (2005), reported that films obtained from banana, okenia and mango starches plasticized with glycerol (starch-to-glycerol weight ratio of 2:1), showed high water solubility values, above 50 %. They used a different film formation procedure based on thermal and cold gelatinization. They concluded that these films could find interesting applications as edible films and candy wrap edible films, as other carboxymethylated starch films. Therefore, the films obtained in this work could also find use in these applications due to the high water solubility values.

3.3. Morphological properties

The morphology of the cross-section of cryofractured samples of the MKF/glycerol films was studied by FESEM. Fig. 3 shows the FESEM images of the films at 1000 × magnification. It can be seen in Fig. 3**a** the presence of MKF particles, which before processing were initially between 600 and 500 μm large, embedded in the glycerol matrix with quite a large gap between the particles and the matrix. This is ascribed to a certain lack of adhesion of MKF particles in the film, which could be due to the large size of the starch-based particles leading to inhomogeneity within the film structure. A similar morphology was observed by Melo et al. (2019), in mango kernel starch (MKS) films with MKF, which presented a great concentration of discontinuities. The black spots found in the films could be ascribed to the presence of lipid globules. These discontinuities are responsible for the low mechanical response observed in the mechanical properties section. It can be appreciated how a decrease in the particle size leads to smaller gaps between the MKF particles and the glycerol matrix. This can be clearly

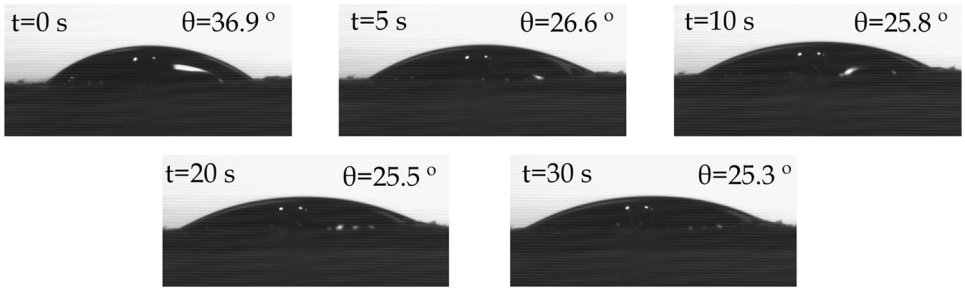

Fig. 2. Evolution of the water contact angle of a distilled water drop onto the surface of MKF-500/400 film over time.

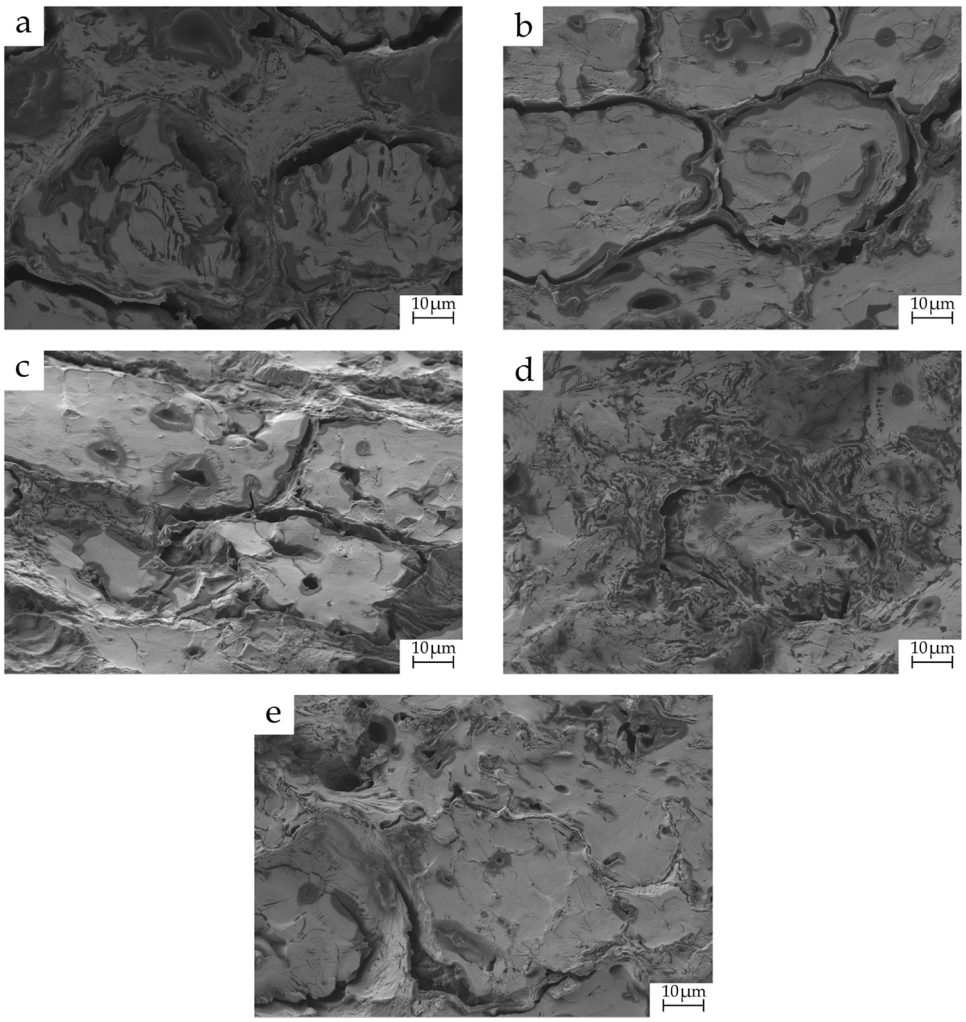

Fig. 3. FESEM images at 1000 × magnification of the MKF/glycerol films: a) MKF-600/500; b) MKF-500/400; c) MKF-400/300; d) MKF-300/200 and e) MKF-200/100.

observed in Figs. 3**d** and 3**e**, where the particles are strongly embedded in the glycerol matrix, especially in the case of the film with 200–100 μm particle size, which presents an almost inexistent gap. Additionally, a superior homogeneity in the surface of the cryofractured films is also seen, which directly relates to the higher mechanical performance of MKF-300/200 and MKF-200/100 films, respectively. This homogeneity and the absence of voids in the film matrix also results in increased barrier properties as can be observed and will be discussed.

It is important to note that, after processing, the MKF particles decrease their size, as it can be observed in the FESEM images. This is due to a partial solubility of the lignocellulosic MKF particles in water, thus, reducing their size (Käldström et al., 2014). In order to expose this phenomenon, Fig. 4 shows the distribution of particle sizes in each one of the films. As it was expected, for smaller initial particle sizes, smaller final particle sizes were obtained. The film with particles between 600 and 500 μm presented an average final particle size of 42.5 μm, while the film with initial particles between 200 and 100 μm exhibited an average particle size of 15 μm. Therefore, it can be said that there is a certain correlation between the initial size of the particles and the final size of the particles in the film.

3.4. Barrier properties

Fig. 5 shows the WVTR value of MKF/glycerol films. It can be observed how the WVTR of the films decreases as the MKP particle size decreases. The WVTR value for MKF-600/500 is $6.9 \cdot 10^5$ g μm/cm^2 day; while the WVTR value for MKF-200/100 is $3.7 \cdot 10^5$ g μm/cm^2 day. This represents a reduction of 46 % in terms of WVTR, which is a remarkable improvement. Smaller particle size leads to higher water affinity in the films as a result of an enhanced starch-based surface area, which should increase WVTR. However, in this case the prevailing phenomenon seems to be an increase in the density of the structure of the films, as a result of a more homogeneous distribution of the particles due to their smaller size. Consequently, WVTR decreases with the size of the particles, as the tortuosity of the diffusion path of water molecules through the film becomes higher (Rojas-Lema et al., 2021). Melo et al. (2019), observed how MKF was capable of reducing the water vapor permeability of MKF/glycerol films, ascribing this effect to the hydrophobic fat content in the particles. These results perfectly match the findings observed in FESEM images, where the homogeneity was observed to increase as the particle size was reduced. It has been also shown that water vapor permeability can be controlled and drastically reduced by reducing the particle size of MKF, which can prove to be an advantage for food packaging and coatings (Melo et al., 2019).

3.5. Visual aspect and color properties

Table 5 shows the main colorimetric parameters and the color co-ordinates of the CieLab cromatic space for all the films herein developed. Additionally, Fig. 6 shows the visual aspect of all the MKF/glycerol

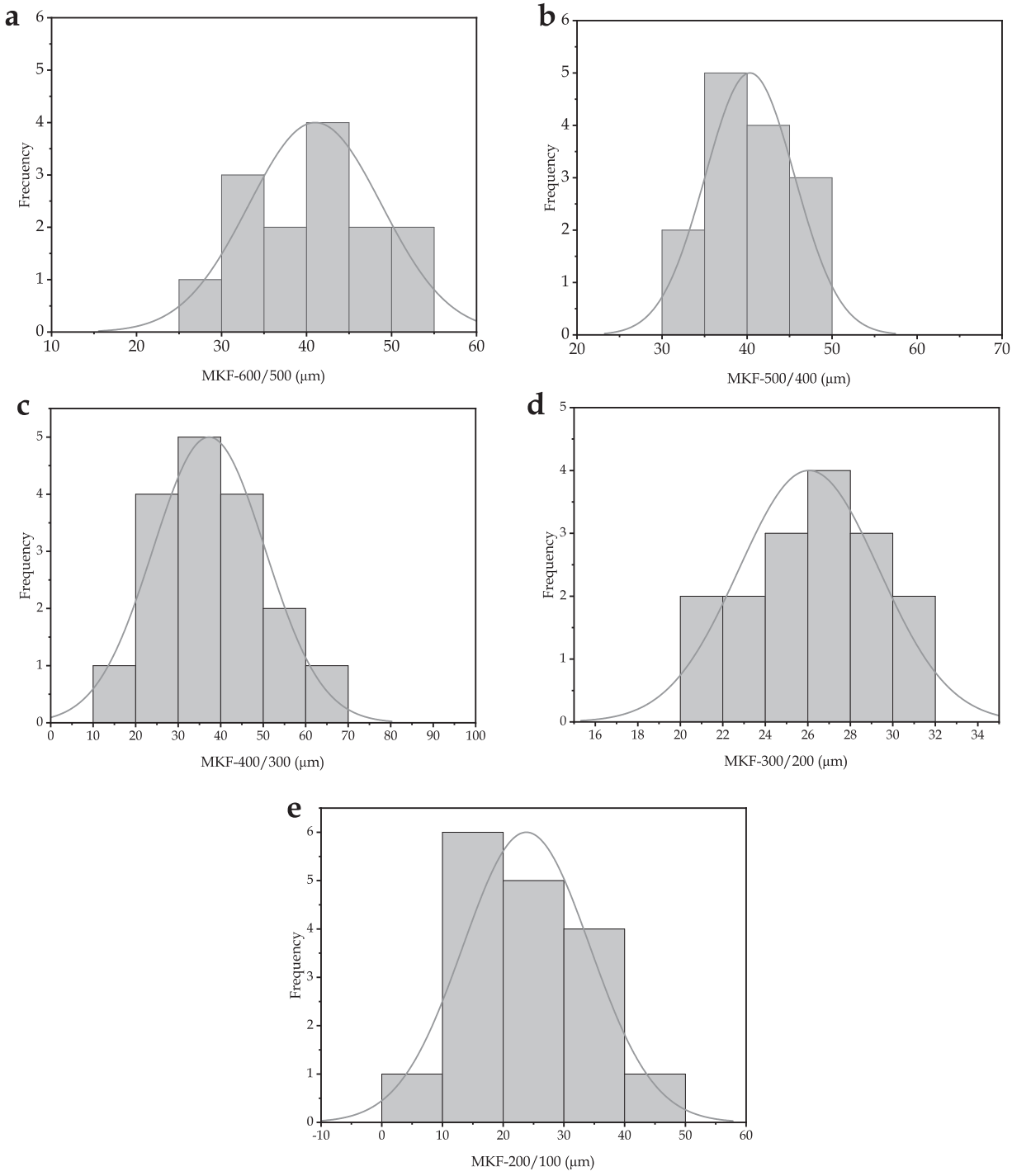

Fig. 4. Histograms of the MKF particles in the films after processing: a) MKF-600/500; b) MKF-500/400; c) MKF-400/300; d) MKF-300/200 e) MKF-200/100.

films. At first sight, it can be seen how all the films present very similar colors between them, with very similar ΔE values. Additionally, they lack any sign of transparency, due to the intrinsic dark color of the MKF particles. Nonetheless On the other hand, it can be observed that luminance (L^*), which is related to the lightness of the samples, decreases with the particle size, which was expected, as smaller particles lead to more homogeneous films and thus, darker colors. This can be confirmed in Fig. 6, where MKF-200/100 exhibits a unique dark brown color, while samples MKF-600/500, MKF-500/400 and MKF-400/300 show signs of heterogeneity, with clearer tonalities in certain areas.

With regard to color coordinate a^*, it stands for green (negative) and red (positive) colors (Jorda-Reolid et al., 2021). The a^* coordinate seems to decrease with the particle size, which could be ascribed to the fact that larger particle samples lead to more heterogeneous films, and show signs of reddish like spots, as it can be seen in Fig. 6, thus leading the a^* value towards more positive values. On the other hand, the b^* coordinate is related to blue (negative) and yellow (positive) colors (Kaur and Kranthi, 2012). In this case, there is a clear difference between the MKF/glycerol films with the three largest particle samples, with values very similar and close to 3.0; and the other two samples, with lower values, close to 2.0. This is mainly ascribed to the fact that the first samples have reddish-yellow like areas (rich in glycerol) as a result of their heterogeneity, while the other two samples lack these areas due to being more homogeneous and thus, decreasing the b^* coordinate value.

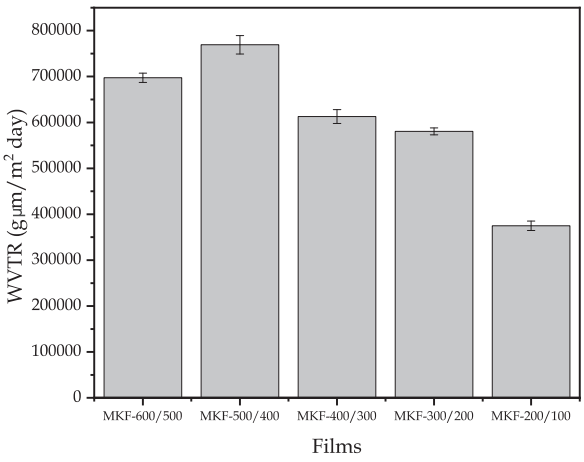

Fig. 5. Water vapor transmission rate (WVTR) of MKF/glycerol films with different particle size.

Table 5
Luminance (L^*), color coordinates (a^*b^*) and total color difference (ΔE) of MKF/glycerol films with different MKF particle size.

Code	L^*	a^*	b^*	ΔE
MKF-600/500	26.2 ± 0.1^a	3.41 ± 0.10^a	3.01 ± 0.08^a	69.2 ± 0.2^a
MKF-500/400	25.8 ± 0.2^a	3.26 ± 0.38^a	3.03 ± 0.16^a	69.5 ± 0.5^a
MKF-400/300	25.7 ± 0.1^a	3.03 ± 0.37^b	3.02 ± 0.15^a	69.6 ± 0.4^a
MKF-300/200	25.2 ± 0.1^a	2.47 ± 0.06^c	2.15 ± 0.15^b	70.1 ± 0.2^a
MKF-200/100	25.2 ± 0.1^a	2.72 ± 0.12^d	2.22 ± 0.14^b	70.0 ± 0.2^a

a–d Different letters in the same column indicate a significant difference ($p < 0.05$).

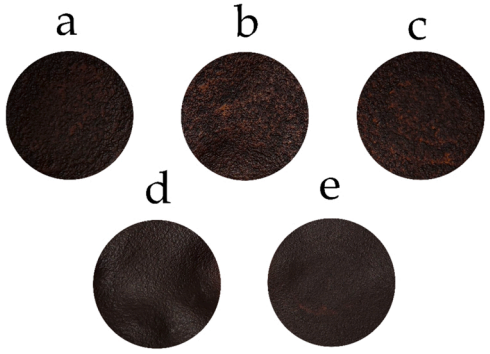

Fig. 6. Visual aspect of MKF/glycerol films: a) MKF-600/500; b) MKF-500/400; c) MKF-400/300; d) MKF-300/200 and e) MKF-200/100.

3.6. Antioxidant activity

DPPH free radical method was used in this study to evaluate the antioxidant activity of the MKF/glycerol films. In this technique, solutions present an initial purple color, that changes into yellow when antioxidant substances are present in the sample. This change in color is based on antioxidants donating hydrogens from their phenolic hydroxyl groups to scavenge free radicals of DPPH and form more stable compounds (Pimpley and Murthy, 2021). Fig. 7 shows the DPPH inhibition (%) profile for all the developed films at different times, from 1 h to 168 h of exposure of the samples to the DPPH solution. It can be seen how all the samples present a very high antioxidant activity (between 85 % and 95 %), compared to other antioxidant films with active compounds such as epigallocatechin gallate nanocapsules (Liang et al., 2017), tea extracts (Lei et al., 2019; Wu et al., 2019), licorice waste

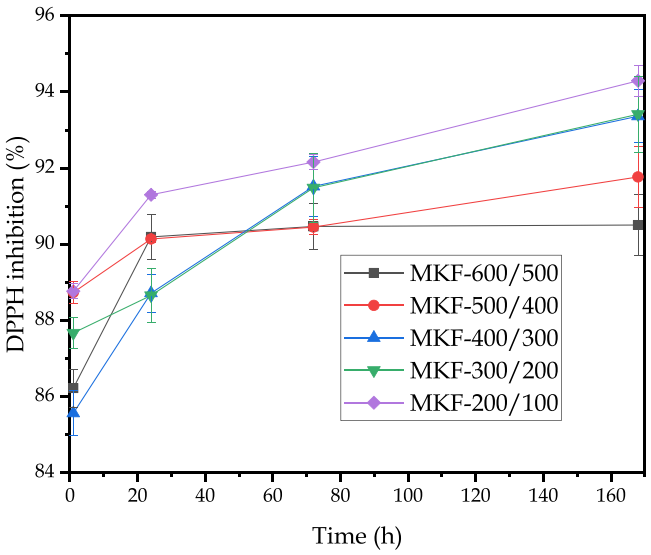

Fig. 7. Percentage of 2.2-diphenyl-1-picrylhydrazyl radical (DPPH) inhibition of MKF/glycerol films with different particle sizes of MKF.

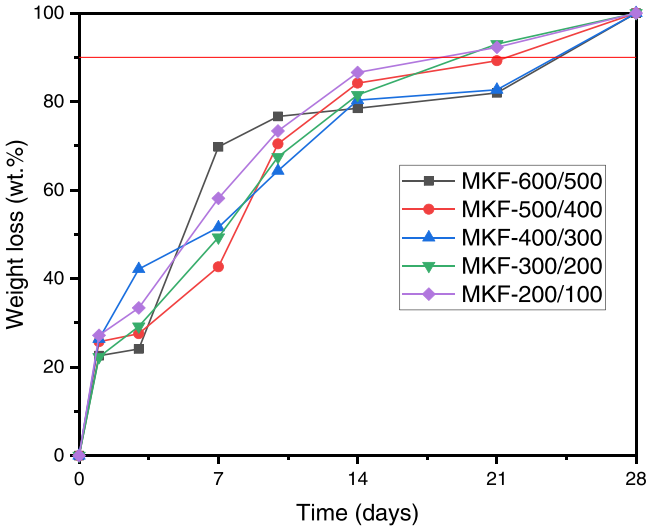

Fig. 8. Biodegradation profile under controlled compost soil in terms of the incubation time of all the MKF/glycerol films with different MKF particle size.

extract (Han et al., 2018) and even mango peel extracts (Adilah et al., 2018a). Melo et al. (2019), reported a similar antioxidant activity, superior to 90 % for films with mango kernel phenolic extracts and mango kernel flour. It can be observed how the radical scavenging activity increases with a decrease in the particle size, being the MKF-200/100 film the one with the highest DPPH inhibition in all the time range, achieving almost 95 % at 168 h. This could be ascribed to the fact that lower particle size leads to a major interface area of the MKF particles with the DPPH solution, thus presenting higher disponibility of hydroxyl groups to donate hydrogens into the DPPH solution (Prasedya et al., 2021). Additionally, it should be noted the rate with which these films achieve their maximum DPPH inhibition, as at only 1 h of the test, this parameter is almost at its maximum, with small variations along the following week until 168 h. Adilah et al. (2018b), also observed a DPPH inhibition of almost 90 % for samples with 5 wt% of mango kernel extract. Nonetheless the results presented here show exceptional radical scavenging activity.

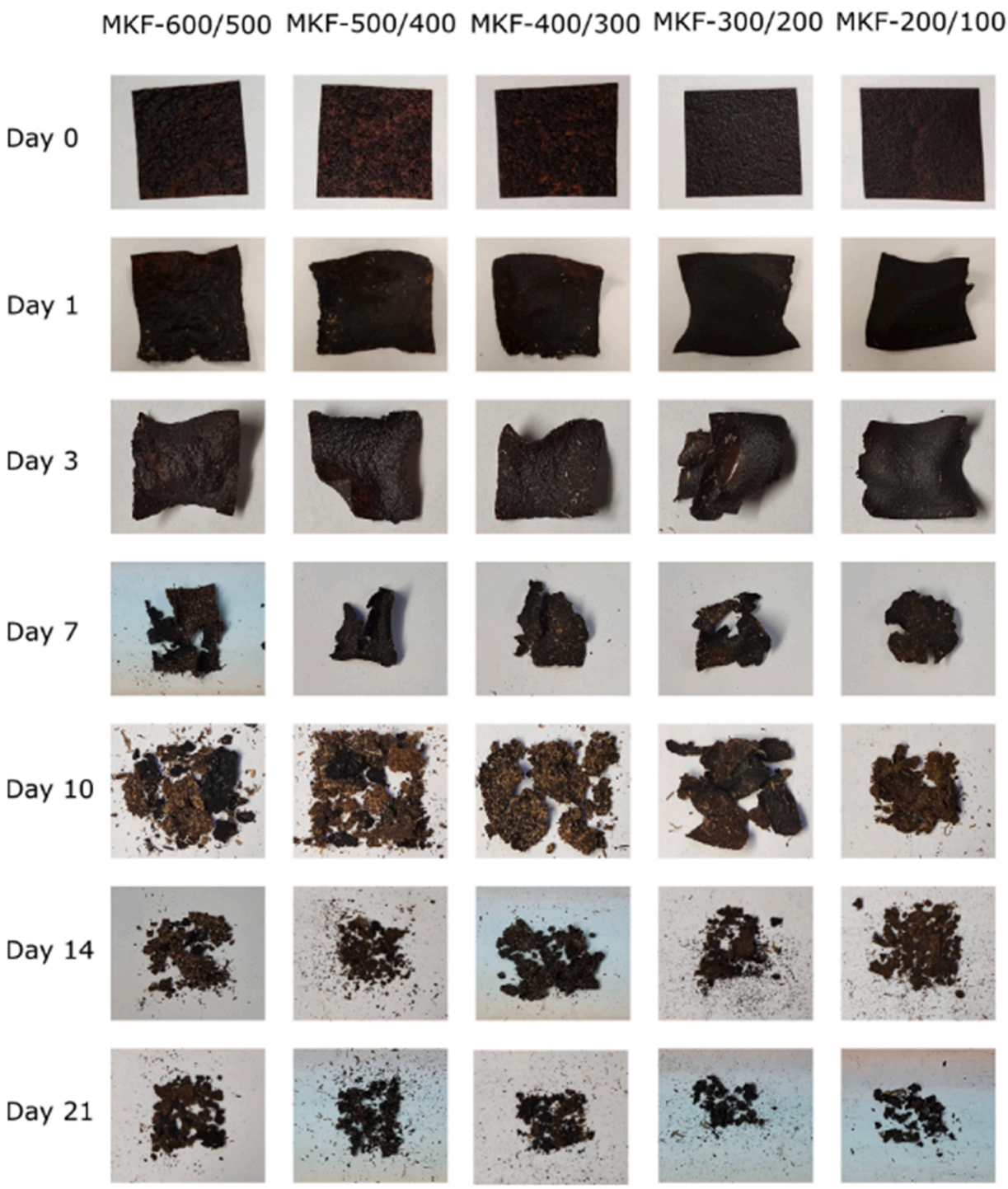

Fig. 9. Visual appearance of the disintegration process of MKF/glycerol films over time with different MKF particle size.

3.7. Disintegration test

The biodegradability of the films was studied by means of the disintegration test. Fig. 8 shows the quantitative evolution of the weight of the samples over time through the disintegration process during 28 days (the red line indicates 90 %, which is the disintegration goal), while Fig. 9 shows the visual appearance of the film samples all over this process. It can be seen how the disintegration profile of all the samples is quite similar in terms of the weight loss rate. All the films strongly disintegrate at the first day of the test, losing more than 20 % of their mass just after that short period of time. This is a sign of the high biodegradability ot these films. Moreover, all the samples completely disintegrate after 28 days of incubation in compost soil, which is another indicator of their degradability under these conditions. The disintegration profile is similar to the one observed by Seligra et al. (2016), in starch/glycerol films, which were disintegrated in 30 days. This behavior is mainly ascribed to the high hydrophilicity that those films possess, as water diffusses into the polymeric film sample causing swelling and increasing microbial growth. In spite of the fact that all the films have a similar disintegration profile, the samples with smaller MKF particle size present a slightly higher biodegradation rate, as they achieve 90 % of disintegration (which is the weight loss goal for considering

Table 6
Arithmetic roughness (R_a) of the MKF/glycerol films with different MKF particle size.

Film	Roughness R_a (μm)
MKF-600/500	17.38 ± 0.08^a
MKF-500/400	16.10 ± 1.10^b
MKF-400/300	13.10 ± 0.76^c
MKF-300/200	7.52 ± 0.22^d
MKF-200/100	6.42 ± 0.53^e

a–e Different letters in the same column indicate a significant difference ($p < 0.05$).

a material biodegradable according to the standard mentioned in the experimental section) faster than the rest of the samples. This could be ascribed to a higher hydrophilic surface of these samples, as shown in wettability and contact angle measurements. This disintegration profile can be confirmed by its visual appearance, which clearly shows how at day 7, the films become very brittle and start to decompose. It can also be seen that at day 21, all the films have suffered strong disintegration, especially samples MKF-300/200 and MKF-200/100, which are almost completely gone.

These results confirm the total biodegradability of these films, as well as their high biodegradation rate in comparison with other biodegradable polymers such as PHB or TPS (Garcia-Garcia et al., 2018; Pavon et al., 2021), whose disintegration time is superior to 40 days. This fact gives MKF/glycerol films of great applicability in environmentally friendly packaging.

3.8. Roughness measurements

The surface topography of the films was studied and evaluated through roughness measurements. Table 6 gathers the mean roughness values (R_a) of all the films. The roughness of the MKF-600/500 film was 17.38 μm, which represents a considerable rough surface in comparison with glycerol and starch films, which show values of 3.0 nm (Villacrés et al., 2014). This is clearly due to the large size of MKF compared to neat starch films. Observing the mean roughness values of all MKF/glycerol films, there is a clear decreasing trend of R_a with a decrease in the size of the MKF particles. Particularly, MKF-300/200 and MKF-200/100 show the lowest roughness, with values of 7.52 and 6.42 μm, respectively. This decreasing tendency is ascribed to an increase in the homogeneity of the surface of the films as a result of the presence of smaller particles, which make an efficient dispersion easier and avoid the formation of MKF aggregates that alter the smoothness of the film surface. These results are in accordance with what was observed in Fig. 6, where the heterogeneity of samples with higher particle size was observed.

4. Conclusions

Totally natural, biodegradable and environmentally friendly glycerol films with mango kernel flour (MKF) of different sizes, ranging from 600 to 100 μm, were successfully obtained by the casting solution method. The obtained films showed an increasing trend in their mechanical properties as the particle size diminished, with a tensile strength and elongation at break of 1.08 MPa and 18.1 %, respectively, for the MKF-200/100 sample. These results were in accordance with FESEM images, which showed that smaller particles lead to more homogeneous structures within the film. Additionally, narrower gaps between the starch-based particles and the glycerol matrix were observed, positively affecting the cohesion of the films and, thus, the mechanical performance as well. The decrease in the particle size of the MKF also improved the barrier properties of the films due to a more homogeneous surface, which increases the density of the film and difficults water vapor to pass through its pores. The MKF-200/100 sample exhibited a WVTR of $3.7 \cdot 10^5$ g μm/cm^2 day, which is 46 % smaller than the WVTR of the MKF-600/500 film. The developed films showed very dark brown colors, which were due to the intrinsic natural color of mango kernel, and they proved to possess a remarkable DPPH radical scavenging capability. Interestingly, just after 1 h of the DPPH test, the films had almost achieved their maximum DPPH inhibition (over 90 % DPPH radical scavenging), which demonstrates their strong antioxidant nature, which is a favorable characteristic in the field of food packaging. The films were also subjected to the disintegration test in controlled compost soil, where they proved to be completely biodegradable, achieving 100 % of weight loss just after 28 days of incubation time. The samples with smaller particles presented a superior biodegradation rate, which may be an interesting feature for food packaging and coating applications. Finally, the roughness of the samples demonstrated that the homogeneity of their surfaces increases as the particle size decreases. The MKF-200/100 film showed the lowest roughness of them all, with a R_a of 6.42 μm.

All in all, the presented results show that the overall properties of the MKF/glycerol films improve when the particle size of MKF decreases, as the structure of the film becomes more homogeneous. This also demonstrates that some properties, such as water vapor permeability, can be controlled through the particle size. Moreover, this fact could be applicable to other films with different starch-based fillers. The herein developed films have proved to be suitable for applications were completely biodegradable, antioxidant and natural films are required.

CRediT authorship contribution statement

J. Gomez-Caturla: Investigation, Writing – original draft, Conceptualization. **J. Ivorra-Martinez:** Formal analysis, Methodology, Visualization. **L. Quiles-Carrillo:** Project administration, Validation, Resources. **R. Balart:** Funding acquisition, Supervision, Writing – review & editing. **D. Garcia-Garcia:** Supervision, Validation, Project administration. **F. Dominici:** Visualization, Data curation, Formal analysis. **D. Puglia:** Software, Resources, Methodology. **L. Torre:** Supervision, Writing – review & editing, Validation.

Declaration of Competing Interest

The authors declare that they have no known competing financial interests or personal relationships that could have appeared to influence the work reported in this paper.

Data Availability

Data will be made available on request.

Acknowledgements

This research is a part of the Grant PID2020-116496RB-C22 funded by MCIN/AEI/10.13039/501100011033. Authors also thank Generalitat Valenciana-GVA, Grant no. AICO/2021/025 and CIGE/2021/094 for supporting this work. J. Gomez-Caturla wants to thank Generalitat Valenciana-GVA, for his FPI grant (ACIF/2021/185) and Grant FPU20/01732 funded by MCIN/AEI/10.13039/501100011033 and by ESF Investing in your future. J. Ivorra-Martinez wants to thank FPU19/01759 Grant funded by MCIN/AEI/10.13039/501100011033 and by ESF Investing in your future. Microscopy Services at UPV are also acknowledged by their help in collecting and analyzing images.

References

Adilah, A.N., Jamilah, B., Noranizan, M., Hanani, Z.N., 2018a. Utilization of mango peel extracts on the biodegradable films for active packaging. Food Packag. Shelf Life 16, 1–7.

Adilah, Z.M., Jamilah, B., Hanani, Z.N., 2018b. Functional and antioxidant properties of protein-based films incorporated with mango kernel extract for active packaging. Food Hydrocoll. 74, 207–218.

Adjei-Fremah, S., Worku, M., De Erive, M.O., He, F., Wang, T., Chen, G., 2019. Effect of microfluidization on microstructure, protein profile and physicochemical properties of whole cowpea flours. Innov. Food Sci. Emerg. Technol. 57, 102207.
Augustin, M., Ling, E., 1987. Composition of Mango Seed Kernel. Pertanika (Malaysia).
Bally, I.S., Bombarely, A., Chambers, A.H., Cohen, Y., Dillon, N.L., Innes, D.J., Islas-Osuna, M.A., Kuhn, D.N., Mueller, L.A., Ophir, R., 2021. The 'Tommy Atkins' mango genome reveals candidate genes for fruit quality. BMC Plant Biol. 21, 1–18.
Bamdad, F., Goli, A.H., Kadivar, M., 2006. Preparation and characterization of proteinous film from lentil (Lens culinaris): edible film from lentil (Lens culinaris). Food Res. Int. 39, 106–111.
Basiak, E., Lenart, A., Debeaufort, F., 2018. How glycerol and water contents affect the structural and functional properties of starch-based edible films. Polymers 10, 412.
Cheng, L.H., Karim, A.A., Seow, C.C., 2006. Effects of water-glycerol and water-sorbitol interactions on the physical properties of konjac glucomannan films. J. Food Sci. 71, E62–E67.
Colla, E., do Amaral Sobral, P.J., Menegalli, F.C., 2006. Amaranthus cruentus flour edible films: influence of stearic acid addition, plasticizer concentration, and emulsion stirring speed on water vapor permeability and mechanical properties. J. Agric. Food Chem. 54, 6645–6653.
Dick, M., Henrique Pagno, C., Haas Costa, T.M., Gomaa, A., Subirade, M., de Oliveira Rios, A., Hickmann Flôres, S., 2016. Edible films based on chia flour: Development and characterization. J. Appl. Polym. Sci. 133.
Garcia-Garcia, D., Lopez-Martinez, J., Balart, R., Strömberg, E., Moriana, R., 2018. Reinforcing capability of cellulose nanocrystals obtained from pine cones in a biodegradable poly (3-hydroxybutyrate)/poly (ε-caprolactone)(PHB/PCL) thermoplastic blend. Eur. Polym. J. 104, 10–18.
Ghiasi, F., Golmakani, M.-T., Eskandari, M.H., Hosseini, S.M.H., 2020. A new approach in the hydrophobic modification of polysaccharide-based edible films using structured oil nanoparticles. Ind. Crops Prod. 154, 112679.
Giosafatto, C.V.L., Al-Asmar, A., D'Angelo, A., Roviello, V., Esposito, M., Mariniello, L., 2018. Preparation and characterization of bioplastics from grass pea flour cast in the presence of microbial transglutaminase. Coatings 8, 435.
Godbillot, L., Dole, P., Joly, C., Rogé, B., Mathlouthi, M., 2006. Analysis of water binding in starch plasticized films. Food Chem. 96, 380–386.
Grinberg, V.Y., Tolstoguzov, V., 1997. Thermodynamic incompatibility of proteins and polysaccharides in solutions. Food Hydrocoll. 11, 145–158.
Han, Y., Yu, M., Wang, L., 2018. Preparation and characterization of antioxidant soy protein isolate films incorporating licorice residue extract. Food Hydrocoll. 75, 13–21.
Hassan, B., Chatha, S.A.S., Hussain, A.I., Zia, K.M., Akhtar, N., 2018. Recent advances on polysaccharides, lipids and protein based edible films and coatings: a review. Int. J. Biol. Macromol. 109, 1095–1107.
Huntrakul, K., Yoksan, R., Sane, A., Harnkarnsujarit, N., 2020. Effects of pea protein on properties of cassava starch edible films produced by blown-film extrusion for oil packaging. Food Packag. Shelf Life 24, 100480.
Jang, Y.-C., Lee, G., Kwon, Y., Lim, J.-h, Jeong, J.-h, 2020. Recycling and management practices of plastic packaging waste towards a circular economy in South Korea. Resour. Conserv. Recycl. 158, 104798.
Jorda-Reolid, M., Gomez-Caturla, J., Ivorra-Martinez, J., Stefani, P.M., Rojas-Lema, S., Quiles-Carrillo, L., 2021. Upgrading argan shell wastes in wood plastic composites with biobased polyethylene matrix and different compatibilizers. Polymers 13, 922.
Käldström, M., Meine, N., Farès, C., Rinaldi, R., Schüth, F., 2014. Fractionation of 'water-soluble lignocellulose'into C5/C6 sugars and sulfur-free lignins. Green Chem. 16, 2454–2462.
Kaur, A., Kranthi, B., 2012. Comparison between YCbCr color space and CIELab color space for skin color segmentation. Int. J. Appl. Inf. Syst. 3, 30–33.
Kocabaş, D.S., Akçelik, M.E., Bahçegül, E., Özbek, H.N., 2021. Bulgur bran as a biopolymer source: production and characterization of nanocellulose-reinforced hemicellulose-based biodegradable films with decreased water solubility. Ind. Crops Prod. 171, 113847.
Lei, Y., Wu, H., Jiao, C., Jiang, Y., Liu, R., Xiao, D., Lu, J., Zhang, Z., Shen, G., Li, S., 2019. Investigation of the structural and physical properties, antioxidant and antimicrobial activity of pectin-konjac glucomannan composite edible films incorporated with tea polyphenol. Food Hydrocoll. 94, 128–135.
Li, W., Xu, Z., Wang, Z., Xing, J., 2018. One-step quaternization/hydroxypropylsulfonation to improve paste stability, adhesion, and film properties of oxidized starch. Polymers 10, 1110.
Liang, J., Yan, H., Zhang, J., Dai, W., Gao, X., Zhou, Y., Wan, X., Puligundla, P., 2017. Preparation and characterization of antioxidant edible chitosan films incorporated with epigallocatechin gallate nanocapsules. Carbohydr. Polym. 171, 300–306.
Liminana, P., Garcia-Sanoguera, D., Quiles-Carrillo, L., Balart, R., Montanes, N., 2018. Development and characterization of environmentally friendly composites from poly (butylene succinate) (PBS) and almond shell flour with different compatibilizers. Compos. Part B: Eng. 144, 153–162.
Masamba, K., Li, Y., Hategekimana, J., Liu, F., Ma, J., Zhong, F., 2016. Effect of Gallic acid on mechanical and water barrier properties of zein-oleic acid composite films. J. Food Sci. Technol. 53, 2227–2235.
Melo, P.E., Silva, A.P.M., Marques, F.P., Ribeiro, P.R., Brito, E.S., Lima, J.R., Azeredo, H. M., 2019. Antioxidant films from mango kernel components. Food Hydrocoll. 95, 487–495.
Mikus, M., Galus, S., Ciurzyńska, A., Janowicz, M., 2021. Development and characterization of novel composite films based on soy protein isolate and oilseed flours. Molecules 26, 3738.
Mokrejs, P., Langmaier, F., Janacova, D., Mladek, M., Kolomaznik, K., Vasek, V., 2009. Thermal study and solubility tests of films based on amaranth flour starch–protein hydrolysate. J. Therm. Anal. Calorim. 98, 299–307.
Nawab, A., Alam, F., Hasnain, A., 2017. Mango kernel starch as a novel edible coating for enhancing shelf-life of tomato (Solanum lycopersicum) fruit. Int. J. Biol. Macromol. 103, 581–586.
Nouraddini, M., Esmaiili, M., Mohtarami, F., 2018. Development and characterization of edible films based on eggplant flour and corn starch. Int. J. Biol. Macromol. 120, 1639–1645.
Pavon, C., Aldas, M., López-Martínez, J., Hernández-Fernández, J., Arrieta, M.P., 2021. Films based on thermoplastic starch blended with pine resin derivatives for food packaging. Foods 10, 1171.
Pérez-Gago, M.B., Krochta, J.M., 2001. Lipid particle size effect on water vapor permeability and mechanical properties of whey protein/beeswax emulsion films. J. Agric. Food Chem. 49, 996–1002.
Pimpley, V.A., Murthy, P.S., 2021. Influence of green extraction techniques on green coffee: nutraceutical compositions, antioxidant potential and in vitro bio-accessibility of phenolics. Food Biosci. 43, 101284.
Prasedya, E., Frediansyah, A., Martyasari, N., Ilhami, B., Abidin, A., Padmi, H., Juanssilfero, A., Widyastuti, S., Sunarwidhi, A., 2021. Effect of particle size on phytochemical composition and antioxidant properties of Sargassum cristaefolium ethanol extract. Sci. Rep. 11, 1–9.
Quiles-Carrillo, L., Montanes, N., Lagaron, J.M., Balart, R., Torres-Giner, S., 2019. Bioactive multilayer polylactide films with controlled release capacity of gallic acid accomplished by incorporating electrospun nanostructured coatings and interlayers. Appl. Sci. 9, 533.
Rojas-Lema, S., Nilsson, K., Trifol, J., Langton, M., Gomez-Caturla, J., Balart, R., Garcia-Garcia, D., Moriana, R., 2021. Faba bean protein films reinforced with cellulose nanocrystals as edible food packaging material. Food Hydrocoll. 121, 107019.
Romero-Bastida, C.A., Bello-Pérez, L.A., García, M.A., Martino, M.N., Solorza-Feria, J., Zaritzky, N.E., 2005. Physicochemical and microstructural characterization of films prepared by thermal and cold gelatinization from non-conventional sources of starches. Carbohydr. Polym. 60, 235–244.
Rosenbloom, R.A., Zhao, Y., 2021. Hydroxypropyl methylcellulose or soy protein isolate-based edible, water-soluble, and antioxidant films for safflower oil packaging. J. Food Sci. 86, 129–139.
Ryan, B.J., Poduska, K.M., 2008. Roughness effects on contact angle measurements. Am. J. Phys. 76, 1074–1077.
Seligra, P.G., Jaramillo, C.M., Famá, L., Goyanes, S., 2016. Biodegradable and non-retrogradable eco-films based on starch–glycerol with citric acid as crosslinking agent. Carbohydr. Polym. 138, 66–74.
Shen, M., Huang, W., Chen, M., Song, B., Zeng, G., Zhang, Y., 2020. (Micro) plastic crisis: un-ignorable contribution to global greenhouse gas emissions and climate change. J. Clean. Prod. 254, 120138.
Silva, A.P.M., Oliveira, A.V., Pontes, S.M., Pereira, A.L., Rosa, M.F., Azeredo, H.M., 2019. Mango kernel starch films as affected by starch nanocrystals and cellulose nanocrystals. Carbohydr. Polym. 211, 209–216.
Tapia-Blácido, D., do Amaral Sobral, P., Menegalli, F., 2011. Optimization of amaranth flour films plasticized with glycerol and sorbitol by multi-response analysis. LWT-Food Sci. Technol. 44, 1731–1738.
Thakor, N., 2019. Indian mango–production and export scenario. Peach, 18, 0.12.
Tonyali, B., Cikrikci, S., Oztop, M.H., 2018. Physicochemical and microstructural characterization of gum tragacanth added whey protein based films. Food Res. Int. 105, 1–9.
Trifol, J., Plackett, D., Sillard, C., Szabo, P., Bras, J., Daugaard, A.E., 2016. Hybrid poly (lactic acid)/nanocellulose/nanoclay composites with synergistically enhanced barrier properties and improved thermomechanical resistance. Polym. Int. 65, 988–995.
Villacrés, R.A.E., Flores, S.K., Gerschenson, L.N., 2014. Biopolymeric antimicrobial films: study of the influence of hydroxypropyl methylcellulose, tapioca starch and glycerol contents on physical properties. Mater. Sci. Eng.: C 36, 108–117.
Vogler, E.A., 1998. Structure and reactivity of water at biomaterial surfaces. Adv. Colloid Interface Sci. 74, 69–117.
Wang, W., Gu, F., Deng, Z., Zhu, Y., Zhu, J., Guo, T., Song, J., Xiao, H., 2021a. Multilayer surface construction for enhancing barrier properties of cellulose-based packaging. Carbohydr. Polym. 255, 117431.
Wang, Y., Meng, Y., Ji, Z., Meng, X., Song, X., Lu, P., Chen, F., 2021b. Bioinspired colored degradable starch-based films with excellent tensile strength. Ind. Crops Prod. 167, 113525.
Wu, H., Lei, Y., Zhu, R., Zhao, M., Lu, J., Xiao, D., Jiao, C., Zhang, Z., Shen, G., Li, S., 2019. Preparation and characterization of bioactive edible packaging films based on pomelo peel flours incorporating tea polyphenol. Food Hydrocoll. 90, 41–49.
Yatnatti, S., Vijayalakshmi, D., Chandru, R., 2014. Processing and nutritive value of mango seed kernel flour. Curr. Res. Nutr. Food Sci. J. 2, 170–175.
Zhang, S., Xia, C., Dong, Y., Yan, Y., Li, J., Shi, S.Q., Cai, L., 2016. Soy protein isolate-based films reinforced by surface modified cellulose nanocrystal. Ind. Crops Prod. 80, 207–213.